



CHORUS

This is the accepted manuscript made available via CHORUS. The article has been published as:

Precision Measurement of the $(e^{\{+\}}+e^{\{-}})$ Flux in Primary Cosmic Rays from 0.5 GeV to 1 TeV with the Alpha Magnetic Spectrometer on the International Space Station

M. Aguilar *et al.* (AMS Collaboration)

Phys. Rev. Lett. **113**, 221102 — Published 26 November 2014

DOI: [10.1103/PhysRevLett.113.221102](https://doi.org/10.1103/PhysRevLett.113.221102)

1 **Precision Measurement of the ($e^+ + e^-$) Flux in Primary Cosmic**
2 **Rays from 0.5 GeV to 1 TeV with the Alpha Magnetic**
3 **Spectrometer on the International Space Station**

4 M. Aguilar,²⁶ D. Aisa,^{33,34} B. Alpat,³³ A. Alvino,³³ G. Ambrosi,³³ K. Andeen,²² L. Arruda,²⁴
5 N. Attig,²¹ P. Azzarello,^{33,16,a} A. Bachlechner,¹ F. Barao,²⁴ A. Barrau,¹⁷ L. Barrin,¹⁵
6 A. Bartoloni,³⁸ L. Basara,^{3,37} M. Battarbee,⁴⁴ R. Battiston,^{37,b} J. Bazo,^{33,c} U. Becker,⁹
7 M. Behlmann,⁹ B. Beischer,¹ J. Berdugo,²⁶ B. Bertucci,^{33,34} G. Bigongiari,^{35,36} V. Bindi,¹⁹
8 S. Bizzaglia,³³ M. Bizzarri,^{33,34} G. Boella,^{28,29} W. de Boer,²² K. Bollweg,²⁰ V. Bonnivard,¹⁷
9 B. Borgia,^{38,39} S. Borsini,³³ M.J. Boschini,²⁸ M. Bourquin,¹⁶ J. Burger,⁹ F. Cadoux,¹⁶
10 X.D. Cai,⁹ M. Capell,⁹ S. Caroff,³ J. Casaus,²⁶ V. Cascioli,³³ G. Castellini,¹⁴ I. Cernuda,²⁶
11 F. Cervelli,³⁵ M.J. Chae,⁴⁰ Y.H. Chang,¹⁰ A.I. Chen,⁹ H. Chen,⁹ G.M. Cheng,⁶ H.S. Chen,⁶
12 L. Cheng,⁴¹ A. Chikanian,^{32,d} H.Y. Chou,¹⁰ E. Choumilov,⁹ V. Choutko,⁹ C.H. Chung,¹
13 C. Clark,²⁰ R. Clavero,²³ G. Coignet,³ C. Consolandi,¹⁹ A. Contin,^{7,8} C. Corti,¹⁹ B. Coste,³⁷
14 M. Crispoltoni,^{33,34} Z. Cui,⁴¹ M. Dai,⁵ C. Delgado,²⁶ S. Della Torre,²⁸ M.B. Demirköz,²
15 L. Derome,¹⁷ S. Di Falco,³⁵ L. Di Masso,^{33,34} F. Dimiccoli,³⁷ C. Díaz,²⁶ P. von Doetinchem,¹⁹
16 F. Donnini,^{33,34} W.J. Du,⁴¹ M. Duranti,³³ D. D'Urso,³³ A. Eline,⁹ F.J. Eppling,⁹ T. Eronen,⁴⁴
17 Y.Y. Fan,^{43,e} L. Farnesini,³³ J. Feng,^{3,f} E. Fiandrini,^{33,34} A. Fiasson,³ E. Finch,³² P. Fisher,⁹
18 Y. Galaktionov,⁹ G. Gallucci,^{35,15} B. García,²⁶ R. García-López,²³ C. Gargiulo,¹⁵ H. Gast,¹
19 I. Gebauer,²² M. Gervasi,^{28,29} A. Ghelfi,¹⁷ W. Gillard,¹⁰ F. Giovacchini,²⁶ P. Goglov,⁹
20 J. Gong,³¹ C. Goy,³ V. Grabski,²⁷ D. Grandi,²⁸ M. Graziani,^{33,15} C. Guandalini,^{7,8}
21 I. Guerri,^{35,36} K.H. Guo,¹⁸ M. Habiby,¹⁶ S. Haino,^{10,43} K.C. Han,²⁵ Z.H. He,¹⁸ M. Heil,⁹
22 J. Hoffman,¹⁰ T.H. Hsieh,⁹ Z.C. Huang,¹⁸ C. Huh,¹³ M. Incagli,³⁵ M. Ionica,³³ W.Y. Jang,¹³
23 H. Jinchi,²⁵ K. Kanishev,³⁷ G.N. Kim,¹³ K.S. Kim,¹³ Th. Kirn,¹ R. Kossakowski,³
24 O. Kounina,⁹ A. Kounine,⁹ V. Koutsenko,⁹ M.S. Krafczyk,⁹ S. Kunz,²² G. La Vacca,^{28,15}
25 E. Laudi,^{33,34,g} G. Laurenti,^{7,8} I. Lazzizzera,³⁷ A. Lebedev,⁹ H.T. Lee,⁴³ S.C. Lee,⁴³
26 C. Leluc,¹⁶ H.L. Li,^{43,h} J.Q. Li,³¹ Q. Li,³¹ Q. Li,^{9,i} T.X. Li,¹⁸ W. Li,⁴ Y. Li,^{16,f} Z.H. Li,⁶
27 Z.Y. Li,^{43,f} S. Lim,⁴⁰ C.H. Lin,⁴³ P. Lipari,³⁸ T. Lippert,²¹ D. Liu,⁴³ H. Liu,³¹ T. Lomtadze,³⁵
28 M.J. Lu,^{37,j} Y.S. Lu,⁶ K. Luebelsmeyer,¹ F. Luo,⁴¹ J.Z. Luo,³¹ S.S. Lv,¹⁸ R. Majka,³²
29 A. Malinin,¹² C. Mañá,²⁶ J. Marín,²⁶ T. Martin,²⁰ G. Martínez,²⁶ N. Masi,^{7,8} D. Maurin,¹⁷
30 A. Menchaca-Rocha,²⁷ Q. Meng,³¹ D.C. Mo,¹⁸ L. Morescalchi,^{35,k} P. Mott,²⁰ M. Müller,¹
31 J.Q. Ni,¹⁸ N. Nikonov,²² F. Nozzoli,^{33,c} P. Nunes,²⁴ A. Obermeier,¹ A. Oliva,²⁶ M. Orcinha,²⁴
32 F. Palmonari,^{7,8} C. Palomares,²⁶ M. Paniccia,¹⁶ A. Papi,³³ M. Pauluzzi,^{33,34} E. Pedreschi,³⁵
33 S. Pensotti,^{28,29} R. Pereira,^{24,19} F. Pilo,³⁵ A. Piluso,^{33,34} C. Pizzolotto,^{33,c} V. Plyaskin,⁹
34 M. Pohl,¹⁶ V. Poireau,³ E. Postaci,² A. Putze,³ L. Quadrani,^{7,8} X.M. Qi,¹⁸ T. Rähä,¹
35 P.G. Rancoita,²⁸ D. Rapin,¹⁶ J.S. Ricol,¹⁷ I. Rodríguez,²⁶ S. Rosier-Lees,³ A. Rozhkov,⁹
36 D. Rozza,²⁸ R. Sagdeev,¹¹ J. Sandweiss,³² P. Saouter,¹⁶ C. Sbarra,^{7,8} S. Schael,¹
37 S.M. Schmidt,²¹ D. Schuckardt,²² A. Schulz von Dratzig,¹ G. Schwering,¹ G. Scolieri,³³
38 E.S. Seo,¹² B.S. Shan,⁴ Y.H. Shan,⁴ J.Y. Shi,³¹ X.Y. Shi,^{9,1} Y.M. Shi,⁴² T. Siedenburger,¹
39 D. Son,¹³ F. Spada,³⁸ F. Spinella,³⁵ W. Sun,⁹ W.H. Sun,^{9,m} M. Tacconi,^{28,29} C.P. Tang,¹⁸
40 X.W. Tang,⁶ Z.C. Tang,⁶ L. Tao,³ D. Tescaro,²³ Samuel C.C. Ting,⁹ S.M. Ting,⁹
41 N. Tomassetti,¹⁷ J. Torsti,⁴⁴ C. Türkoğlu,² T. Urban,²⁰ V. Vagelli,²² E. Valente,^{38,39}
42 C. Vannini,³⁵ E. Valtonen,⁴⁴ S. Vaurynovich,⁹ M. Vecchi,^{3,n} M. Velasco,²⁶ J.P. Vialle,³
43 L.Q. Wang,⁴¹ Q.L. Wang,⁵ R.S. Wang,⁴² X. Wang,⁹ Z.X. Wang,¹⁸ Z.L. Weng,⁹

44 K. Whitman,¹⁹ J. Wienkenhöver,¹ H. Wu,³¹ X. Xia,^{26, h} M. Xie,^{9, i} S. Xie,⁴² R.Q. Xiong,³¹
45 G.M. Xin,⁴¹ N.S. Xu,¹⁸ W. Xu,^{6, 9} Q. Yan,⁶ J. Yang,⁴⁰ M. Yang,⁶ Q.H. Ye,⁴² H. Yi,³¹ Y.J. Yu,⁵
46 Z.Q. Yu,⁶ S. Zeissler,²² J.H. Zhang,³¹ M.T. Zhang,¹⁸ X.B. Zhang,¹⁸ Z. Zhang,¹⁸ Z.M. Zheng,⁴
47 H.L. Zhuang,⁶ V. Zhukov,¹ A. Zichichi,^{7, 8} N. Zimmermann,¹ P. Zuccon,⁹ and C. Zurbach³⁰

(AMS Collaboration)

48
49 ¹*I. Physics Institute and JARA-FAME, RWTH*
50 *Aachen University, D-52056 Aachen, Germany^o*

51 ²*Department of Physics, Middle East Technical University (METU), 06800 Ankara, Turkey^p*

52 ³*Laboratoire d'Annecy-Le-Vieux de Physique des Particules (LAPP),*
53 *IN2P3/CNRS and Université de Savoie, F-74941 Annecy-le-Vieux, France*

54 ⁴*Beihang University (BUAA), Beijing, 100191, China*

55 ⁵*Institute of Electrical Engineering (IEE), Chinese*
56 *Academy of Sciences, Beijing, 100080, China*

57 ⁶*Institute of High Energy Physics (IHEP), Chinese*
58 *Academy of Sciences, Beijing, 100039, China^a*

59 ⁷*INFN-Sezione di Bologna, I-40126 Bologna, Italy^f*

60 ⁸*Università di Bologna, I-40126 Bologna, Italy*

61 ⁹*Massachusetts Institute of Technology (MIT), Cambridge, Massachusetts 02139, USA*

62 ¹⁰*National Central University (NCU), Chung-Li, Tao Yuan 32054, Taiwan^s*

63 ¹¹*East-West Center for Space Science, University*
64 *of Maryland, College Park, Maryland 20742, USA*

65 ¹²*IPST, University of Maryland, College Park, Maryland 20742, USA*

66 ¹³*CHEP, Kyungpook National University, 702-701 Daegu, Korea^t*

67 ¹⁴*CNR-IROE, I-50125 Firenze, Italy*

68 ¹⁵*European Organization for Nuclear Research (CERN), CH-1211 Geneva 23, Switzerland*

69 ¹⁶*DPNC, Université de Genève, CH-1211 Genève 4, Switzerland*

70 ¹⁷*Laboratoire de Physique subatomique et de cosmologie (LPSC),*
71 *CNRS/IN2P3 and Université Grenoble-Alpes, F-38026 Grenoble, France*

72 ¹⁸*Sun Yat-Sen University (SYSU), Guangzhou, 510275, China*

73 ¹⁹*Physics and Astronomy Department, University of Hawaii,*
74 *2505 Correa Road, WAT 432; Honolulu, Hawaii 96822, USA*

75 ²⁰*National Aeronautics and Space Administration Johnson Space*
76 *Center (JSC), and Jacobs-Sverdrup, Houston, Texas 77058, USA*

77 ²¹*Jülich Supercomputing Centre and JARA-FAME,*
78 *Research Centre Jülich, D-52425 Jülich, Germanyⁿ*

79 ²²*Institut für Experimentelle Kernphysik, Karlsruhe Institute*
80 *of Technology (KIT), D-76128 Karlsruhe, Germany^r*

81 ²³*Instituto de Astrofísica de Canarias (IAC), E-38205, La Laguna, Tenerife, Spain*

82 ²⁴*Laboratório de Instrumentação e Física Experimental*
83 *de Partículas, (LIP), P-1000 Lisboa, Portugal*

84 ²⁵*National Chung-Shan Institute of Science and*
85 *Technology (NCSIST), Longtan, Tao Yuan 325, Taiwan*

86 ²⁶*Centro de Investigaciones Energéticas, Medioambientales*
87 *y Tecnológicas (CIEMAT) E-28040 Madrid, Spain^w*

88 ²⁷*Instituto de Física, Universidad Nacional Autónoma*
89 *de México (UNAM), México, D. F., 01000 México^x*

90
91
92
93
94
95
96
97
98
99
100
101
102
103
104
105
106
107
108

²⁸*INFN-Sezione di Milano–Bicocca, I-20126 Milano, Italy*^f

²⁹*Università di Milano–Bicocca, I-20126 Milano, Italy*

³⁰*Laboratoire Univers et Particules de Montpellier (LUPM), IN2P3/CNRS
and Université de Montpellier II, F-34095 Montpellier, France*

³¹*Southeast University (SEU), Nanjing, 210096, China*

³²*Physics Department, Yale University, New Haven, Connecticut 06520, USA*

³³*INFN-Sezione di Perugia, I-06100 Perugia, Italy*^f

³⁴*Università di Perugia, I-06100 Perugia, Italy*

³⁵*INFN-Sezione di Pisa, I-56100 Pisa, Italy*^f

³⁶*Università di Pisa, I-56100 Pisa, Italy*

³⁷*INFN–TIFPA and Università di Trento, I-38123 Povo, Trento, Italy*^f

³⁸*INFN-Sezione di Roma 1, I-00185 Roma, Italy*^f

³⁹*Università di Roma La Sapienza, I-00185 Roma, Italy*

⁴⁰*Department of Physics, Ewha Womans University, Seoul, 120-750, Korea*^y

⁴¹*Shandong University (SDU), Jinan, Shandong, 250100, China*

⁴²*Shanghai Jiaotong University (SJTU), Shanghai, 200030, China*

⁴³*Institute of Physics, Academia Sinica, Nankang, Taipei 11529, Taiwan*^s

⁴⁴*Space Research Laboratory, Department of Physics and
Astronomy, University of Turku, FI-20014 Turku, Finland*

Abstract

We present a measurement of the cosmic ray ($e^+ + e^-$) flux in the range 0.5 GeV to 1 TeV based on the analysis of 10.6 million ($e^+ + e^-$) events collected by AMS. The statistics and the resolution of AMS provide a precision measurement of the flux. The flux is smooth and reveals new and distinct information. Above 30.2 GeV, the flux can be described by a single power law with a spectral index $\gamma = -3.170 \pm 0.008(\text{stat.} + \text{syst.}) \pm 0.008(\text{energy scale})$.

109 Measurements of cosmic rays by the Alpha Magnetic Spectrometer (AMS) [1–3] of the
 110 positron fraction and the positron flux $\Phi(e^+)$ have been carried out up to 500 GeV and of the
 111 electron flux $\Phi(e^-)$ up to 700 GeV. The results generated widespread interest and discussions
 112 on the origin of high energy positrons and electrons [4]. They provide information on the
 113 combined flux $\Phi(e^+ + e^-)$ up to 500 GeV. In this Letter we present a dedicated measurement
 114 of $\Phi(e^+ + e^-)$ up to 1 TeV with reduced statistical and systematic errors.

115 *AMS.* — AMS is a general purpose high-energy particle physics detector installed on the
 116 International Space Station (ISS) to conduct a unique long-duration (~ 20 -year) mission of
 117 fundamental physics research in space [5]. It consists of a tracker, a magnet, time of flight
 118 (TOF) and anti-coincidence counters, a ring imaging Čerenkov detector, an electromagnetic
 119 calorimeter (ECAL), and a transition radiation detector (TRD).

120 The nine layer double-sided silicon microstrip tracker accurately determines the trajectory
 121 and absolute charge $|Z|$ of cosmic rays using multiple measurements of the coordinates and
 122 energy loss. Together with the 0.14 T permanent magnet, the tracker measures the particle
 123 rigidity $R = p/Z$, where p is the momentum. The maximum detectable rigidity is 2 TV over
 124 a lever arm of 3 m.

125 The four TOF planes trigger the readout of all the detectors and measure the particle
 126 velocity and direction. The high efficiency ($\simeq 99.999\%$) anti-coincidence counters inside the
 127 magnet bore are used to reject particles outside the geometric acceptance. The tracker,
 128 TOF, and TRD measure $|Z|$ independently. The curvature measured with the tracker and
 129 the magnet and the direction of the particle measured with the TOF yield the sign of the
 130 charge.

131 The 3-dimensional imaging capability of the 17 radiation length ($17X_0$) ECAL allows for
 132 an accurate measurement of the $(e^+ + e^-)$ energy E scaled to the top of AMS and of the
 133 shower shape. An ECAL estimator, based on a boosted decision tree algorithm [6], is used
 134 to differentiate $(e^+ + e^-)$ from protons by exploiting their different shower shapes.

135 To further differentiate between $(e^+ + e^-)$ and protons, signals from the 20 layers of
 136 proportional tubes in the TRD are combined into a TRD classifier formed from the product of
 137 the probabilities of the $(e^+ + e^-)$ hypothesis. This TRD classifier has the same differentiation
 138 power as the TRD likelihood variable used in [3] but has a different scale.

139 The timing, location, and attitude are determined by a combination of GPS units affixed
 140 to AMS and to the ISS. AMS operates continuously on the ISS and is monitored and
 141 controlled around the clock from the ground. The detector performance is steady over time.

142 The entire detector has been extensively calibrated in a test beam at CERN with e^+
 143 and e^- from 10 to 290 GeV/ c , with protons at 180 and 400 GeV/ c , and with π^\pm from 10
 144 to 180 GeV/ c which produce transition radiation equivalent to protons up to 1.2 TeV/ c .
 145 Measurements with 18 different energies and particles at 2000 positions were performed.
 146 A Monte Carlo program based on the GEANT 4.9.4 package [7] is used to simulate physics
 147 processes and detector signals.

148 *Analysis.* — Over 41×10^9 events collected from May 19, 2011 to November 26, 2013 have
 149 been analyzed. The isotropic $(e^+ + e^-)$ flux is measured in each energy bin E , of width ΔE ,
 150 as:

$$\Phi(e^+ + e^-) = \frac{N(E)}{A_{\text{eff}}(E)\epsilon_{\text{trig}}(E)\epsilon_{\text{ECAL}}(E)T(E)\Delta E} \quad (1)$$

151 where N is the number of $(e^+ + e^-)$ events, A_{eff} is the effective detector acceptance, ϵ_{trig} is
 152 the trigger efficiency, ϵ_{ECAL} is the signal selection efficiency based on the ECAL estimator,
 153 and T is the exposure time.

Eqn. (1) is evaluated independently in 74 energy bins from 0.5 GeV to 1 TeV. The bin width is chosen to be at least two times the energy resolution. The bin-to-bin migration error is $\sim 1\%$ at 1 GeV decreasing to 0.2% above 10 GeV. With increasing energy the bin width smoothly increases to ensure adequate statistics in each bin.

The absolute energy scale is verified by using minimum ionizing particles and the ratio E/p . These results are compared with the test beam values where the beam energy is known to high precision. This comparison limits the uncertainty of the absolute energy scale to 2% in the range covered by the test beam results, 10–290 GeV. Below 10 GeV it increases to 5% at 0.5 GeV and above 290 GeV to 5% at 1 TeV. This is treated as an uncertainty on the bin boundaries.

Events are selected requiring the presence of a downward-going, $\beta > 0.83$ particle which has hits in at least 8 of the 20 TRD layers and a single track in the tracker passing through the ECAL. Events with an energy deposition compatible with a minimum ionizing particle in the first $5X_0$ of the ECAL are rejected. Events with $|Z| > 1$ are rejected using dE/dx in the tracker and TRD. Secondary particles of atmospheric origin [8] are rejected with the cutoff requirement discussed below.

In each energy bin, TRD classifier reference spectra of the $(e^+ + e^-)$ signal and the proton background are used as *templates*. The templates are constructed from the data using pure samples of e^- and protons. These samples are selected using the ECAL estimator, E/p matching, and the charge sign. The templates are evaluated separately in each bin, however the signal templates show no dependence on the energy above ~ 10 GeV. Therefore, all the e^- selected in the range 15.1–83.4 GeV are taken as a unique signal template up to the highest energies.

The sum of the signal and background templates is fit to the data by varying their normalizations. This yields the number of signal $(e^+ + e^-)$ events N and the number of background (proton) events. It also yields the statistical errors on N and the number of background events. These errors yield the statistical error on the flux. Figure 1 presents the data, the fit, and the signal and background templates for one bin.

The effective detector acceptance is:

$$A_{\text{eff}} = A_{\text{geom}} \epsilon_{\text{sel}} (1 + \delta) \quad (2)$$

where A_{geom} is the geometric acceptance, ϵ_{sel} is the event selection efficiency, and δ is a data-derived correction. The acceptance for a particle that passes through the active volumes of the tracker, TRD, TOF, and ECAL is found to be $A_{\text{geom}} \simeq 550 \text{ cm}^2 \text{ sr}$ and ϵ_{sel} has typical values of 90% at 10 GeV, 83% at 100 GeV, and 70% at 1 TeV. Both A_{geom} and ϵ_{sel} are evaluated from the Monte Carlo simulation. The small correction to the acceptance δ is estimated by comparing the data and the Monte Carlo simulation efficiencies for every selection cut using information from the detectors unrelated to that cut. This correction is found to be a smooth, slowly varying function of energy. It is -0.04 at 2 GeV and -0.03 at 1 TeV.

The trigger efficiency is determined from data. The data acquisition system is triggered by the coincidence of all four TOF planes. AMS also records unbiased triggers which require a coincidence of any three out of the four TOF planes to measure ϵ_{trig} . It is 100% above 3 GeV decreasing to 75% at 1 GeV.

The ECAL estimator efficiency ϵ_{ECAL} is measured from the data using negative rigidity samples and the selection cuts. ϵ_{ECAL} values range from 75% to 95% for different energy bins, depending on the number of signal and background events.

199 The orbital parameters and the status of the detectors are recorded for each second of
 200 data-taking. Livetime-weighted seconds are summed to obtain the exposure time in a given
 201 energy bin only when the minimum bin energy exceeds 1.2 times the maximum Størmer
 202 cutoff [9] for $|Z| = 1$ particles in the AMS geometric acceptance. The exposure time does
 203 not include time spent in the South Atlantic Anomaly, time during TRD gas refills, and
 204 time when the AMS z axis was more than 40° from the local zenith. For the energy bins
 205 above ~ 30 GeV, where the effects of the geomagnetic cutoff are negligible, the exposure time
 206 is 6.2×10^7 seconds. It decreases to 1.5×10^7 seconds at 5 GeV.

207 A total of 10.6×10^6 ($e^+ + e^-$) events have been identified with energies from 0.5 GeV
 208 to 1 TeV. A major experimental advantage of the combined flux analysis compared to the
 209 measurement of the individual positron and electron fluxes, particularly at high energies,
 210 is that the selection does not depend on the charge sign. Another advantage is that it has
 211 a higher overall efficiency. Consequently, this measurement is extended to 1 TeV with less
 212 overall uncertainty over the entire energy range. Systematic uncertainties arise from (i) the
 213 event selection, (ii) the acceptance, and (iii) bin-to-bin migration.

214 To evaluate the systematic uncertainty from the event selection which includes the un-
 215 certainty from the construction of the templates, 2000 trials were performed in each energy
 216 bin. Each trial consisted of the complete analysis. The trials were performed with different
 217 values of the ECAL estimator cut and different values of selection cuts used to construct
 218 the templates. The 2000 trials are performed in an interval of $\pm 5\%$ in efficiency around the
 219 value of the ECAL estimator cut which minimizes the combined statistical and systematic
 220 uncertainties. For the 500–700 GeV bin, Fig. 2a shows the stability of the number of signal
 221 events corrected by the ECAL estimator selection efficiency $N_E = N/\epsilon_{\text{ECAL}}$ as a function
 222 of ϵ_{ECAL} . As seen, N_E does not depend on the efficiency and this was found to be the case
 223 in every energy bin. Figure 2b shows the distribution of N_E for the 2000 trials in this bin.
 224 The median value of the distribution determines the flux. The RMS spread of the distri-
 225 bution provides an evaluation of the stability of the measurement. The difference between
 226 the width of this distribution in data and the expected statistical fluctuations quantifies the
 227 systematic uncertainty as $<1\%$ below ~ 200 GeV increasing to 4% in the 500–700 GeV bin.
 228 This is the main source of systematic uncertainty above ~ 500 GeV.

229 The systematic error on the acceptance is given by the uncertainty on δ . It is estimated
 230 from data to Monte Carlo simulation comparisons. Above 3 GeV a systematic of 2% on
 231 $(1 + \delta)$ is obtained from the contributions of all the cuts. Below 3 GeV the uncertainty
 232 increases to 6% at 1 GeV. This is the major contribution to the systematic error below
 233 ~ 500 GeV. The systematic error on the acceptance includes a bin-to-bin correlation of 1.4%
 234 over the entire energy range.

235 *Results.*— The measured ($e^+ + e^-$) flux is presented in Table I as a function of the energy
 236 at the top of AMS together with its statistical and systematic errors, where the systematic
 237 errors are the quadratic sum of the systematic uncertainties listed above, (i-iii). The table
 238 also contains a representative value of the energy in the bin, \tilde{E} , for a flux $\propto E^{-3}$ [10] and
 239 the error on \tilde{E} according to the energy scale uncertainty. Several independent analyses were
 240 performed on the same data sample by different study groups. The results of those analyses
 241 are consistent with the results presented here. The flux multiplied by \tilde{E}^3 is presented in
 242 Fig. 3, together with previous measurements [11–17]. Below ~ 10 GeV, the behavior of
 243 $\Phi(e^+ + e^-)$ is affected by solar modulation. However, above 20 GeV the effects of solar
 244 modulation are insignificant within the current experimental accuracy. The data show no
 245 structures. In particular, from 10 GeV to 1 TeV the flux is smooth and reveals new and

246 distinct information.

247 As seen in Fig. 3, the flux cannot be described by a single power law ($\Phi \propto E^\gamma$) over the
248 entire range. To estimate a lower energy limit above which a single power law describes the
249 flux, we use energy intervals with starting energies from 0.5 GeV and increasing bin by bin.
250 The ending energy for all intervals is fixed at 1 TeV. Each interval is split into two sections
251 with a boundary between the starting energy and 1 TeV. Each of the two sections is fit with
252 a single power law and we obtain two spectral indices. The lowest starting energy of the
253 interval that gives consistent spectral indices at the 90% C.L. for any boundary yields a
254 lower limit of 30.2 GeV.

255 To quantitatively examine the energy dependence of the flux in a model independent way,
256 the flux is fit with a spectral index γ as

$$\Phi(e^+ + e^-) = CE^\gamma \quad \text{or} \quad \gamma = d[\log(\Phi)]/d[\log(E)] \quad (3)$$

257 (E in GeV and C is a normalization) over a sliding energy window. The width of the
258 window varies with energy to have sufficient sensitivity to determine the spectral index.
259 The resulting energy dependence of the fitted spectral index is shown in Fig. 4a, where
260 the shading indicates the correlation between neighboring points due to the sliding energy
261 window. Fitting a single power law over the range 30.2 GeV to 1 TeV yields $\gamma = -3.170 \pm$
262 0.008 ± 0.008 where the first error is the combined statistical and systematic uncertainty
263 and the second error is due to the energy scale uncertainty. This is shown in Fig. 4b.

264 It is important to note, as discussed in Ref. [3], that a single power law can describe the
265 electron flux above 52.3 GeV and a single power law, with a different spectral index, can
266 describe the positron flux above 27.2 GeV. The simultaneous single power law behavior of
267 $\Phi(e^+)$, $\Phi(e^-)$, and $\Phi(e^+ + e^-)$ is unexpected.

268 This measurement of $\Phi(e^+ + e^-)$ together with the measurements of $\Phi(e^+)$ and $\Phi(e^-)$ [3]
269 and the positron fraction make possible the accurate comparison with various particle physics
270 and astrophysics models including the minimal model discussed in Ref. [1, 2]. This will be
271 presented in a separate publication.

272 In conclusion, the precision measurement of $\Phi(e^+ + e^-)$ as a function of energy from
273 0.5 GeV to 1 TeV indicates that the flux is smooth and reveals new and distinct information.
274 No structures were observed. From 30.2 GeV to 1 TeV, the flux can be described by a single
275 power law with $\gamma = -3.170 \pm 0.008(\text{stat.} + \text{syst.}) \pm 0.008(\text{energy scale})$.

276 *Acknowledgments.*— We thank former NASA Administrator Daniel S. Goldin for his
277 dedication to the legacy of the ISS as a scientific laboratory and his decision for NASA
278 to fly AMS as a DOE payload. We also acknowledge the support of the NASA leadership
279 including Charles Bolden and William Gerstenmeier. We are grateful for the support of
280 Jim Siegrist and Michael Salamon of the DOE. We also acknowledge the continuous support
281 from M.I.T. and its School of Science, Michael Sipser, Marc Kastner, Ernest Moniz, and
282 Richard Milner. We acknowledge support from: CAS, NNSF, MOST, NLAA, and the
283 provincial governments of Shandong, Jiangsu and Guangdong, China; CNRS, IN2P3, CNES,
284 Enigmass and the ANR, France; J. Trümper, J.D. Woerner, and DLR, Germany; INFN and
285 ASI, Italy; CIEMAT, CDTI, SEIDI-MINECO, and CPAN, Spain; the Swiss National Science
286 Foundation (SNSF), federal and cantonal authorities, Switzerland; and Academia Sinica and
287 the National Science Council (NSC), former President of Academia Sinica Yuan-Tseh Lee
288 and former Ministers of NSC, Maw-Kuen Wu and Luo-Chuan Lee, Taiwan. We gratefully
289 acknowledge the strong support from CERN, including Rolf-Dieter Heuer, and ESA. We are
290 grateful for important discussions with Barry Barish, Jonathan Ellis, Jonathan Feng, Steve

291 Olsen, George Smoot, Michael Turner, Steven Weinberg, and Frank Wilczek. The strong
292 support of the JSC and MSFC flight control teams has allowed AMS to operate optimally
293 on the ISS for over three years.

294 ^a Currently at ISDC, CH–1290 Versoix, Switzerland.

295 ^b Currently at ASI, Rome, I–00133, Italy.

296 ^c Work carried out at the ASI Science Data Center (ASDC) in the framework of the ASI–INFN
297 agreement C/011/11/1.

298 ^d Deceased.

299 ^e Xi’an Jiaotong University, XJTU, Xi’an, 710049, China; and China Scholarship Council.

300 ^f Sun Yat–Sen University (SYSU), Guangzhou, 510275, China; and China Scholarship Council.

301 ^g Currently at European Organization for Nuclear Research (CERN), CH–1211 Geneva 23,
302 Switzerland.

303 ^h Shandong University (SDU), Jinan, Shandong, 250100, China; and China Scholarship Council.

304 ⁱ Harbin Institute of Technology, HIT, Harbin, 150001, China; and China Scholarship Council.

305 ^j University of Science and Technology of China, USTC, Hefei, 230026, China; and China
306 Scholarship Council.

307 ^k and U. Siena, I–53100, Italy.

308 ^l Beijing Normal University, BNU, Beijing, 100875, China; and China Scholarship Council.

309 ^m Southeast University (SEU), Nanjing, 210096, China; and China Scholarship Council.

310 ⁿ Supported by the Centre national d’études spatiales, CNES.

311 ^o Supported by the Deutsches Zentrum für Luft– und Raumfahrt, DLR.; Computing resources
312 from JARA-HPC under project JARA0052.

313 ^p Supported by the Turkish Atomic Energy Authority, TAEK.

314 ^q Supported by the National Natural Science Foundation of China.

315 ^r Also supported by the Italian Space Agency, ASI, contract ASI-INFN I/002/13/0.

316 ^s Also supported by the Ministry of Science and Technology.

317 ^t Grants NRF-2009-0080142, NRF-2012-010226.

318 ^u Computing resources from JARA-HPC under project JARA0052.

319 ^v Supported by the Deutsches Zentrum für Luft– und Raumfahrt, DLR.

320 ^w Also supported by SEIDI and CPAN.

321 ^x Supported by Consejo Nacional de Ciencia y Tecnología, CONACYT.

322 ^y Grant NRF-2013-004883.

323 [1] M. Aguilar *et al.*, Phys. Rev. Lett. **110**, 141102 (2013).

324 [2] L. Accardo *et al.*, Phys. Rev. Lett. **113**, 121101 (2014).

325 [3] M. Aguilar *et al.*, Phys. Rev. Lett. **113**, 121102 (2014).

326 [4] L. Feng R.–Z. Yang, H.–N. He, T.–K. Dong, Y.–Z. Fan, and J. Chang, Phys. Lett. B **728**,
327 250 (2014); K. Blum, B. Katz, and E. Waxman, Phys. Rev. Lett. **111**, 211101 (2013); L.
328 Bergström, T. Bringmann, I. Cholis, D. Hooper, and C. Weniger, Phys. Rev. Lett. **111**,
329 171101 (2013); I. Cholis and D. Hooper, Phys. Rev. D **88**, 023013 (2013); T. Linden and
330 S. Profumo, Astrophys. J. **772**, 18 (2013); R. Cowsik, B. Burch, and T. Madziwa-Nussinov,
331 Astrophys. J. **786**, 124 (2014).

332 [5] A. Kounine, Int. J. Mod. Phys. E**21**, 1230005 (2012); S. Rosier-Lees, in *Proceedings of As-*
333 *troparticle Physics TEVPA/IDM, Amsterdam, 2014* (to be published); S.C.C. Ting, Nucl.

- 334 Phys. B, Proc. Suppl. **243-244**, 12 (2013); S.-C. Lee, in *Proceedings of the 20th International*
335 *Conference on Supersymmetry and Unification of Fundamental Interactions (SUSY 2012),*
336 *Beijing, 2012* (unpublished); M. Aguilar, in *Proceedings of the XL International Meeting on*
337 *Fundamental Physics, Centro de Ciencias de Benasque Pedro Pascual, 2012* (unpublished);
338 S. Schael, in *Proceedings of the 10th Symposium on Sources and Detection of Dark Matter and*
339 *Dark Energy in the Universe, Los Angeles, 2012* (unpublished); B. Bertucci, *Proc. Sci.*, EPS-
340 HEP (2011) 67; M. Incagli, AIP Conf. Proc. **1223**, 43 (2009); R. Battiston, Nucl. Instrum.
341 Methods Phys. Res. Sect. A **588**, 227 (2008).
- 342 [6] B. P. Roe, H.-J. Yang, J. Zhu, Y. Liu, I. Stancu, and G. McGregor, Nucl. Instrum. Methods
343 Phys. Res., Sect. A **543**, 577 (2005).
- 344 [7] J. Allison *et al.*, IEEE Trans. Nucl. Sci. **53**, 270 (2006); S. Agostinelli *et al.*, Nucl. Instrum.
345 Methods Phys. Res., Sect. A **506**, 250 (2003).
- 346 [8] J. Alcaraz *et al.*, Phys. Lett. B **484**, 10 (2000).
- 347 [9] D. Smart and M. Shea, Adv. Sp. Res. **36**, 2012 (2005); C. Størmer, *The Polar Aurora* (Oxford
348 University Press, London, 1950).
- 349 [10] G.D. Lafferty and T.R. Wyatt, Nucl. Instr. Methods Phys. Res., Sect. A **355**, 541 (1995). We
350 have used Eqn (6) with $\tilde{E} \equiv x_{lw}$.
- 351 [11] S. Torii *et al.*, Astrophys. J. **559**, 973 (2001).
- 352 [12] M. A. DuVernois *et al.*, Astrophys. J. **559**, 296 (2001).
- 353 [13] J. Chang *et al.*, Nature (London) **456**, 362 (2008).
- 354 [14] K. Yoshida *et al.*, Adv. in Space Res. **42**, 1670 (2008).
- 355 [15] F. Aharonian *et al.*, Phys. Rev. Lett. **101**, 261104 (2008).
- 356 [16] F. Aharonian *et al.*, Astron. Astrophys. **508**, 561 (2009).
- 357 [17] M. Ackermann *et al.*, Phys. Rev. D **82** 092004 (2010).

TABLE I: The electron plus positron flux $\Phi(e^+ + e^-)$ in units of $[\text{GeV} \cdot \text{m}^2 \cdot \text{sr} \cdot \text{s}]^{-1}$ with its statistical and systematic errors. The systematic uncertainties include an overall scaling uncertainty of 1.4% which introduces a correlation between bins. \tilde{E} as described in the text with its systematic error derived from the energy scale uncertainty. The bin boundaries and \tilde{E} are the energies at the top of AMS.

Energy [GeV]	\tilde{E} [GeV]	$\Phi(e^+ + e^-) \pm \sigma_{\text{stat}} \pm \sigma_{\text{syst}}$
0.50 – 0.65	0.57 ± 0.03	$(2.71 \pm 0.10 \pm 0.54) \times 10^{+1}$
0.65 – 0.82	0.73 ± 0.03	$(2.38 \pm 0.02 \pm 0.21) \times 10^{+1}$
0.82 – 1.01	0.91 ± 0.04	$(2.17 \pm 0.01 \pm 0.16) \times 10^{+1}$
1.01 – 1.22	1.11 ± 0.05	$(2.01 \pm 0.01 \pm 0.12) \times 10^{+1}$
1.22 – 1.46	1.33 ± 0.05	$(1.78 \pm 0.01 \pm 0.09) \times 10^{+1}$
1.46 – 1.72	1.58 ± 0.06	$(1.46 \pm 0.00 \pm 0.06) \times 10^{+1}$
1.72 – 2.00	1.85 ± 0.07	$(1.19 \pm 0.00 \pm 0.04) \times 10^{+1}$
2.00 – 2.31	2.15 ± 0.08	$(9.47 \pm 0.01 \pm 0.28) \times 10^0$
2.31 – 2.65	2.47 ± 0.08	$(7.48 \pm 0.01 \pm 0.19) \times 10^0$
2.65 – 3.00	2.82 ± 0.09	$(5.77 \pm 0.01 \pm 0.13) \times 10^0$
3.00 – 3.36	3.17 ± 0.10	$(4.81 \pm 0.01 \pm 0.10) \times 10^0$
3.36 – 3.73	3.54 ± 0.11	$(3.77 \pm 0.01 \pm 0.08) \times 10^0$
3.73 – 4.12	3.92 ± 0.12	$(2.99 \pm 0.00 \pm 0.06) \times 10^0$
4.12 – 4.54	4.32 ± 0.12	$(2.37 \pm 0.00 \pm 0.05) \times 10^0$
4.54 – 5.00	4.76 ± 0.13	$(1.87 \pm 0.00 \pm 0.04) \times 10^0$
5.00 – 5.49	5.24 ± 0.14	$(1.47 \pm 0.00 \pm 0.03) \times 10^0$
5.49 – 6.00	5.74 ± 0.15	$(1.16 \pm 0.00 \pm 0.02) \times 10^0$
6.00 – 6.54	6.26 ± 0.15	$(9.13 \pm 0.01 \pm 0.19) \times 10^{-1}$
6.54 – 7.10	6.81 ± 0.16	$(7.24 \pm 0.01 \pm 0.15) \times 10^{-1}$
7.10 – 7.69	7.39 ± 0.17	$(5.76 \pm 0.01 \pm 0.12) \times 10^{-1}$
7.69 – 8.30	7.99 ± 0.18	$(4.57 \pm 0.01 \pm 0.09) \times 10^{-1}$
8.30 – 8.95	8.62 ± 0.19	$(3.65 \pm 0.01 \pm 0.07) \times 10^{-1}$
8.95 – 9.62	9.28 ± 0.19	$(2.92 \pm 0.01 \pm 0.06) \times 10^{-1}$
9.62 – 10.32	9.96 ± 0.20	$(2.35 \pm 0.01 \pm 0.05) \times 10^{-1}$
10.3 – 11.0	10.7 ± 0.2	$(1.89 \pm 0.00 \pm 0.04) \times 10^{-1}$
11.0 – 11.8	11.4 ± 0.2	$(1.54 \pm 0.00 \pm 0.03) \times 10^{-1}$
11.8 – 12.6	12.2 ± 0.2	$(1.26 \pm 0.00 \pm 0.03) \times 10^{-1}$
12.6 – 13.4	13.0 ± 0.3	$(1.03 \pm 0.00 \pm 0.02) \times 10^{-1}$
13.4 – 14.2	13.8 ± 0.3	$(8.42 \pm 0.03 \pm 0.17) \times 10^{-2}$
14.2 – 15.1	14.7 ± 0.3	$(6.91 \pm 0.02 \pm 0.14) \times 10^{-2}$
15.1 – 16.1	15.6 ± 0.3	$(5.73 \pm 0.02 \pm 0.12) \times 10^{-2}$
16.1 – 17.0	16.5 ± 0.3	$(4.74 \pm 0.02 \pm 0.10) \times 10^{-2}$
17.0 – 18.0	17.5 ± 0.3	$(3.93 \pm 0.02 \pm 0.08) \times 10^{-2}$
18.0 – 19.0	18.5 ± 0.4	$(3.29 \pm 0.01 \pm 0.07) \times 10^{-2}$
19.0 – 20.0	19.5 ± 0.4	$(2.75 \pm 0.01 \pm 0.06) \times 10^{-2}$
20.0 – 21.1	20.6 ± 0.4	$(2.31 \pm 0.01 \pm 0.05) \times 10^{-2}$

Continued on the next page

TABLE I – *Continued from the previous page*

Energy [GeV]	\bar{E} [GeV]	$\Phi(e^+ + e^-) \pm \sigma_{\text{stat}} \pm \sigma_{\text{syst}}$
21.1 – 22.2	21.7 ± 0.4	(1.94 ± 0.01 ± 0.04) × 10 ⁻²
22.2 – 23.4	22.8 ± 0.5	(1.65 ± 0.01 ± 0.03) × 10 ⁻²
23.4 – 24.6	24.0 ± 0.5	(1.39 ± 0.01 ± 0.03) × 10 ⁻²
24.6 – 25.9	25.2 ± 0.5	(1.19 ± 0.01 ± 0.02) × 10 ⁻²
25.9 – 27.2	26.6 ± 0.5	(9.98 ± 0.06 ± 0.20) × 10 ⁻³
27.2 – 28.7	28.0 ± 0.6	(8.52 ± 0.05 ± 0.17) × 10 ⁻³
28.7 – 30.2	29.4 ± 0.6	(7.22 ± 0.04 ± 0.15) × 10 ⁻³
30.2 – 31.8	31.0 ± 0.6	(6.03 ± 0.04 ± 0.12) × 10 ⁻³
31.8 – 33.5	32.7 ± 0.7	(5.15 ± 0.03 ± 0.11) × 10 ⁻³
33.5 – 35.4	34.4 ± 0.7	(4.29 ± 0.03 ± 0.09) × 10 ⁻³
35.4 – 37.3	36.3 ± 0.7	(3.64 ± 0.03 ± 0.07) × 10 ⁻³
37.3 – 39.4	38.3 ± 0.8	(3.11 ± 0.02 ± 0.06) × 10 ⁻³
39.4 – 41.6	40.5 ± 0.8	(2.59 ± 0.02 ± 0.05) × 10 ⁻³
41.6 – 44.0	42.8 ± 0.9	(2.18 ± 0.02 ± 0.04) × 10 ⁻³
44.0 – 46.6	45.3 ± 0.9	(1.81 ± 0.02 ± 0.04) × 10 ⁻³
46.6 – 49.3	47.9 ± 1.0	(1.49 ± 0.01 ± 0.03) × 10 ⁻³
49.3 – 52.3	50.8 ± 1.0	(1.24 ± 0.01 ± 0.03) × 10 ⁻³
52.3 – 55.6	53.9 ± 1.1	(1.04 ± 0.01 ± 0.02) × 10 ⁻³
55.6 – 59.1	57.3 ± 1.1	(8.62 ± 0.10 ± 0.18) × 10 ⁻⁴
59.1 – 63.0	61.0 ± 1.2	(7.06 ± 0.09 ± 0.15) × 10 ⁻⁴
63.0 – 67.3	65.1 ± 1.3	(5.62 ± 0.07 ± 0.12) × 10 ⁻⁴
67.3 – 72.0	69.6 ± 1.4	(4.56 ± 0.06 ± 0.09) × 10 ⁻⁴
72.0 – 77.4	74.6 ± 1.5	(3.66 ± 0.05 ± 0.08) × 10 ⁻⁴
77.4 – 83.4	80.3 ± 1.6	(2.91 ± 0.04 ± 0.06) × 10 ⁻⁴
83.4 – 90.2	86.7 ± 1.7	(2.32 ± 0.04 ± 0.05) × 10 ⁻⁴
90.2 – 98.1	94.0 ± 1.9	(1.78 ± 0.03 ± 0.04) × 10 ⁻⁴
98 – 107	103 ± 2	(1.37 ± 0.03 ± 0.03) × 10 ⁻⁴
107 – 118	113 ± 2	(1.01 ± 0.02 ± 0.02) × 10 ⁻⁴
118 – 132	125 ± 3	(7.26 ± 0.15 ± 0.15) × 10 ⁻⁵
132 – 149	140 ± 3	(5.04 ± 0.12 ± 0.11) × 10 ⁻⁵
149 – 170	159 ± 3	(3.55 ± 0.09 ± 0.08) × 10 ⁻⁵
170 – 198	183 ± 4	(2.17 ± 0.06 ± 0.05) × 10 ⁻⁵
198 – 237	216 ± 4	(1.27 ± 0.04 ± 0.03) × 10 ⁻⁵
237 – 290	262 ± 5	(6.89 ± 0.27 ± 0.16) × 10 ⁻⁶
290 – 370	327 ± 7	(3.45 ± 0.17 ± 0.09) × 10 ⁻⁶
370 – 500	429 ± 13	(1.45 ± 0.10 ± 0.04) × 10 ⁻⁶
500 – 700	589 ± 22	(5.41 ± 0.56 ± 0.23) × 10 ⁻⁷
700 – 1000	832 ± 38	(1.90 ± 0.40 ± 0.23) × 10 ⁻⁷

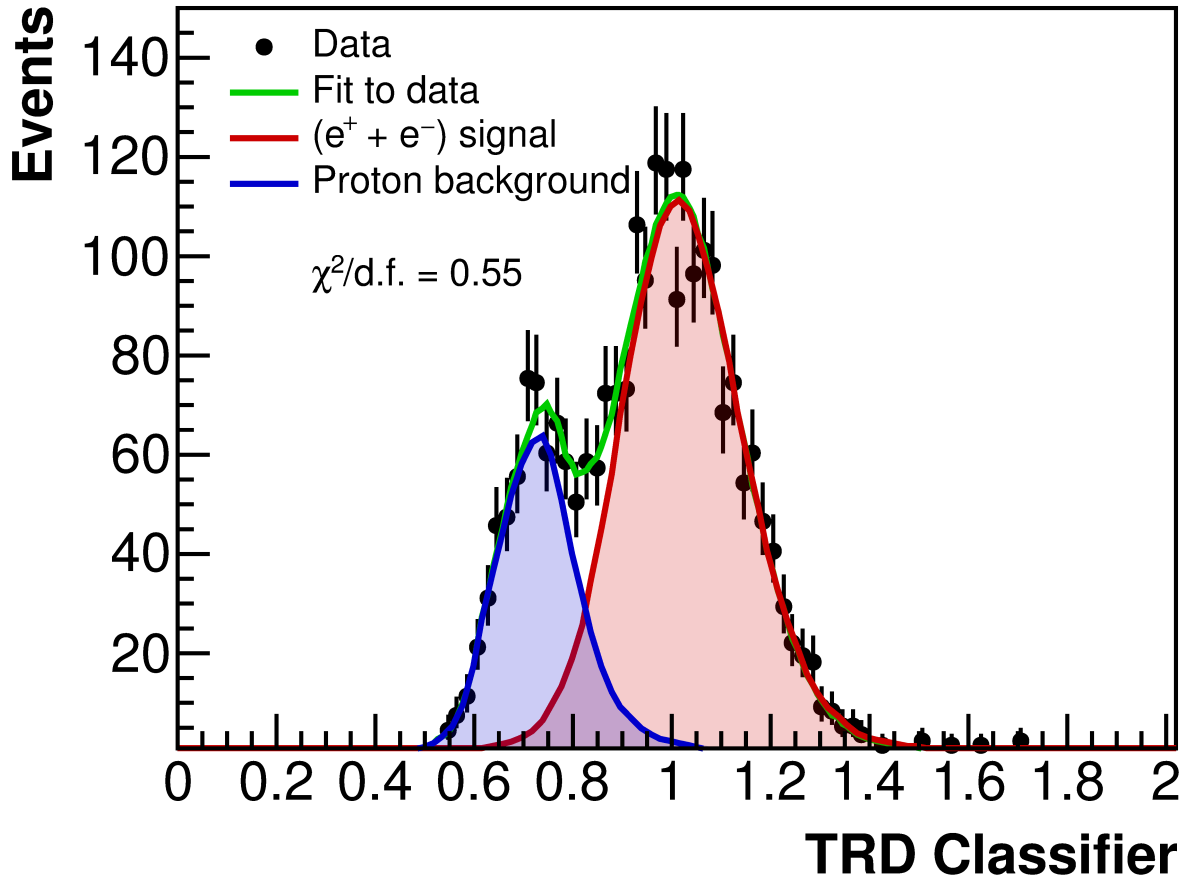


FIG. 1. The result of the template fit in the 149–170 GeV bin showing the small proton background overlapping the $(e^+ + e^-)$ signal. The fit has a $\chi^2/d.f. = 0.55$.

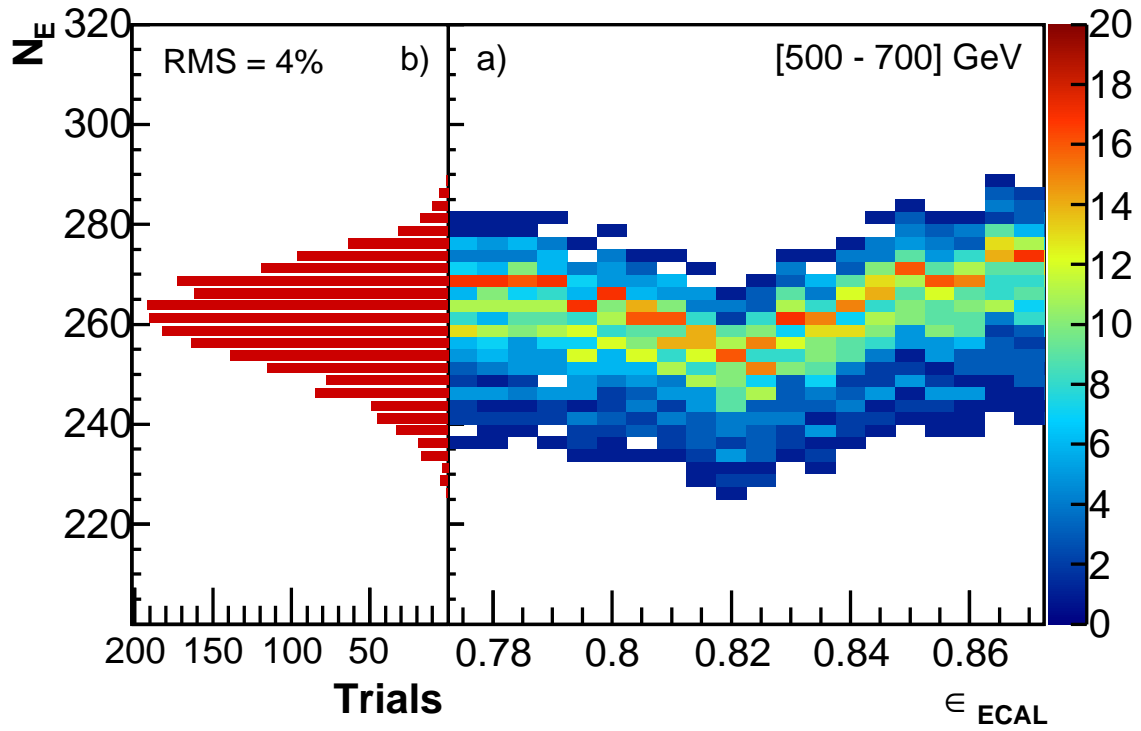


FIG. 2. For the 500–700 GeV bin: (a) N_E versus ϵ_{ECAL} for the 2000 trials showing that the result is stable over a wide range of ϵ_{ECAL} . The scale on the right indicates the number of trials. (b) The distribution of N_E for the 2000 trials. The narrow width (an RMS of 4%) of the distribution indicates the accuracy at the highest energies.

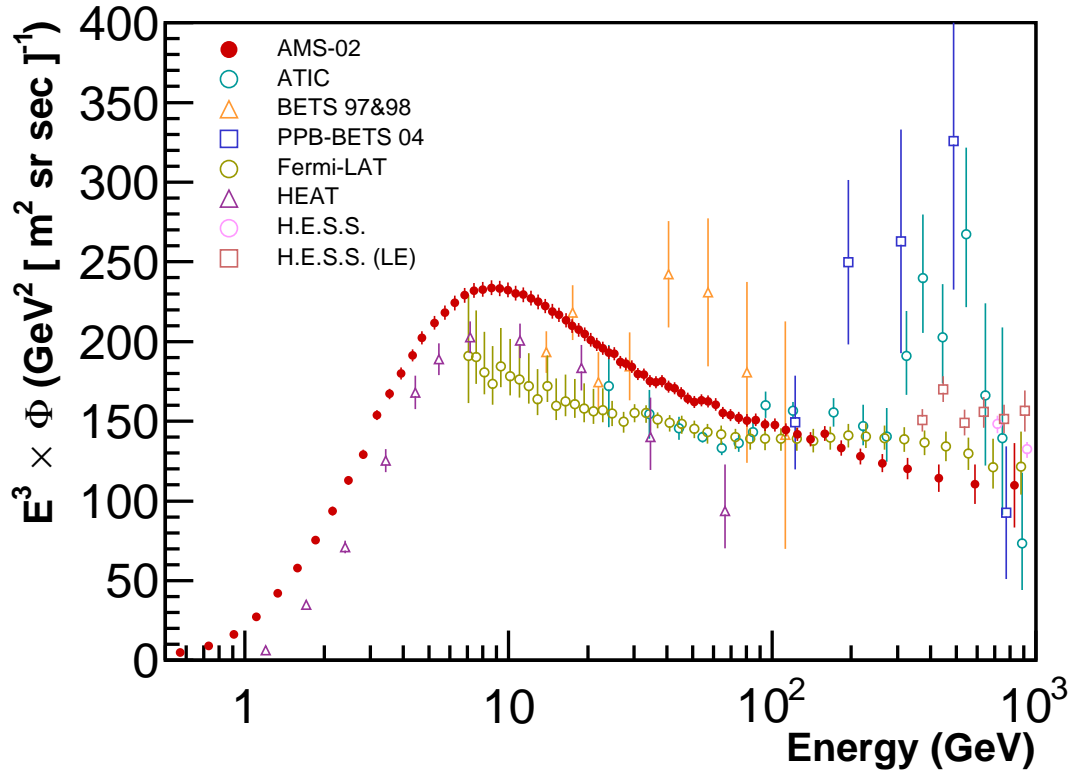


FIG. 3. The flux of electrons plus positrons $\Phi(e^+ + e^-)$ measured by AMS multiplied by \tilde{E}^3 versus energy. The AMS error bars are the quadratic sum of the statistical and systematic errors. Also shown are the results from earlier experiments [11–17].

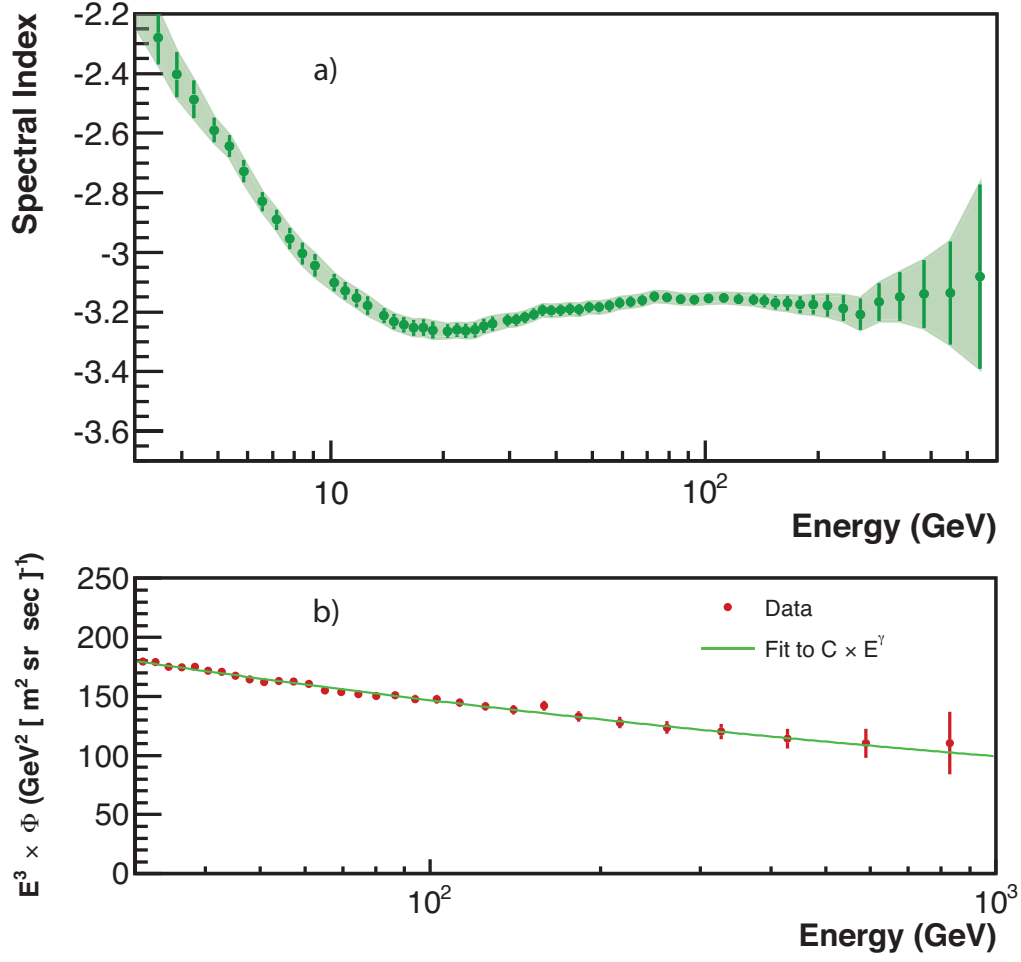


FIG. 4. (a) The spectral index of $\Phi(e^+ + e^-)$ as a function of energy. The shaded regions indicate the 68% C.L. intervals including the correlation between neighboring points due to the sliding energy window. (b) $\Phi(e^+ + e^-)$ multiplied by \tilde{E}^3 versus energy and the result of a single power law fit above 30.2 GeV.